Computers & Fluids 75 (2013) 1–10

Contents lists available at SciVerse ScienceDirect

Computers & Fluids

journal homepage: www.elsevier.com/locate/compfluid

MHD boundary layer flow and heat transfer of a nanofluid past a permeable stretching sheet with velocity, thermal and solutal slip boundary conditions

Wubshet Ibrahim [a,*], Bandari Shankar [b]

[a] Department of Mathematics, Ambo University, Ambo, Ethiopia
[b] Department of Mathematics, Osmania University, Hyderabad 7, Andhra Pradesh, India

ARTICLE INFO

Article history:
Received 9 August 2012
Received in revised form 6 December 2012
Accepted 18 January 2013
Available online 1 February 2013

Keywords:
Nanofluid
Stretching sheet
Slip boundary conditions
Brownian motion
Thermophoresis
Heat transfer

ABSTRACT

In this analysis, the boundary layer flow and heat transfer over a permeable stretching sheet due to a nanofluid with the effects of magnetic field, slip boundary condition and thermal radiation have been investigated. The transport equations used in the analysis took into account the effect of Brownian motion and thermophoresis parameters. The solution for the velocity, temperature and nanoparticle concentration depends on parameters viz. thermal radiation parameter *R*, Prandtl number Pr, Lewis number Le, Brownian motion parameter Nb, thermophoresis parameter Nt, Eckert number Ec, magnetic parameter *M* and slip parameters. Similarity transformation is used to convert the governing non-linear boundary-layer equations into coupled higher order non-linear ordinary differential equations. These equations are numerically solved using fourth order Runge–Kutta method along with shooting technique. An analysis has been carried out to elucidate the effects of governing parameters corresponding to various physical conditions. Numerical results are obtained for distributions of velocity, temperature and concentration, as well as, for the skin friction, local Nusselt number and local Sherwood number for several values of governing parameters. The results indicate that the local Nusselt number decreases with an increase in both Brownian motion parameter Nb and thermophoresis parameter Nt. However, the local Sherwood number increases with an increase in both thermophoresis parameter Nt and Lewis number Le, but it decreases as the values of Nb increase. Besides, it was found that the surface temperature of a sheet increases with an increase in the Eckert number Ec. A comparison with previous studies available in the literature has been done and we found an excellent agreement with it.

1. Introduction

The boundary layer flow over a stretching sheet in a uniform stream of fluid has been studied extensively in fluid mechanics. A large number of research has been done on the area of the boundary layer flow over a moving continuous stretching sheet in the view of its numerous industrial and engineering applications. Some of the wide application areas we have come across are in the aerodynamic extrusion of plastic sheet, in metallurgy, cooling of an infinite metallic plate in a cooling bath, polymer extrusion, cooling or drying of papers and in textile and glass fiber production.

Flow and heat transfer characteristics over a stretching sheet have important industrial applications, for instance, in the extrusion of a polymer sheet from a die. In the manufacturing of such sheets, the melt issues from a slit and is subsequently stretched. The rates of stretching and cooling have a significant influence on the quality of the final product with desired characteristics. The aforementioned processes involve cooling of a molten liquid by drawing into a cooling system. The properties desired for the product of such process mainly depend on two characteristics:the first is the cooling liquid used and the other is the rate of stretching. Liquids of non-Newtonian characteristics with weak electrical conductivity can be chosen for as a cooling liquid as their flow and hence the heat transfer rate can be regulated through some external means. Optimal rate of stretching is important, as rapid stretching results in sudden solidification, thereby destroying the properties expected from the product.

After the pioneering work of Sakiadis [1], a large number of research papers on a stretching sheet have been published by considering various governing parameters such as suction/injection, porosity, magnetic field parameter, and radiation with different types of fluids such as Newtonian, non-Newtonian, polar, and couple stress fluids. However, the abundant literature on the boundary

* Corresponding author. Tel.: +251 911892494.
E-mail addresses: wubshetib@yahoo.com (W. Ibrahim), bandarishanker@yahoo.co.in (B. Shankar).

0045-7930/$ - see front matter © 2013 Elsevier Ltd. All rights reserved.
http://dx.doi.org/10.1016/j.compfluid.2013.01.014

Nomenclature

A	velocity slip parameter
B	thermal slip parameter
C	solutal slip parameter
c_f	skin friction coefficient
D_B	Brownian diffusion coefficient
D_T	thermophoresis diffusion coefficient
f	dimensionless stream function
k	thermal conductivity
Le	Lewis number
M	magnetic parameter
Nb	Brownian motion parameter
Nt	thermophoresis parameter
Nu_x	local Nusselt number
Pr	Prandtl number
R	thermal radiation parameter
Re_x	local Reynolds number
T	temperature of the fluid inside the boundary layer
Sh_x	local Sherwood number
T_w	uniform temperature over the surface of the sheet
T_∞	ambient temperature
u, v	velocity component along x- and y-direction

Greek symbols

η	dimensionless similarity variable
μ	dynamic viscosity of the fluid
υ	kinematic viscosity of the fluid
ϕ	dimensionless concentration function
ρ_f	density of the fluid
$(c\rho)_f$	heat capacity of the fluid
$(c\rho)_p$	effective heat capacity of a nanoparticle
ψ	stream function
α	thermal diffusivity
θ	dimensionless temperature
τ	parameter defined by $\frac{(c\rho)_p}{(c\rho)_f}$

Subscripts

∞	condition at the free stream
w	condition at the surface

layer flow over a stretching sheet is limited to Newtonian and some non-Newtonian fluids flow with traditional no-slip flow boundary condition over various stretching geometry such as linear and non-linear stretching sheet and a little attention was given to stretching sheet with slip boundary condition. However, fluids with micro-scale or nano-scale dimensions have flow behavior that greatly differs from the traditional fluid flow characteristics and belongs to the slip flow regime. For the flow in the slip regime, the fluid motion still obeys the Navier–Stoke's equations, but with slip velocity, temperature and concentration boundary conditions. For instance, the flow in many applications of micro/nano systems such as hard disk drive, micro-pump, micro-valve and micro-nozzles is in slip transition regime, which is characterized by slip boundary at the wall.

The no-slip boundary condition is known as the main manifestation of the Navier–Stoke's theory of fluid dynamics. But there are situations wherein such condition is not appropriate. Especially no-slip condition is inadequate for most non-Newtonian liquids and nanofluids, as some polymer melt often shows microscopic wall slip and that in general is governed by a non-linear and monotone relation between the slip velocity and the traction. The liquids exhibiting boundary slip find applications in technological problems such as polishing of artificial heart valves and internal cavities.

The earlier studies that took into account the slip boundary condition over a stretching sheet were conducted by Andersson [2]. He gave a closed form solution of a full Navier–Stokes equations for a magnetohydrodynamics flow over a stretching sheet. Following Andersson, Wang [3] found the closed form similarity solution of a full Navier–Stoke's equations for the flow due to a stretching sheet with partial slip. Furthermore, Wang [4] investigated stagnation slip flow and heat transfer on a moving plate. Similarly, Fang et al. [5] studied slip magnetohydrodynamics viscous flow over a stretching sheet analytically. Still further, Hayat et al. [6] expanded the problem of the previous researchers by incorporating thermal slip condition and discussed unsteady magneto hydrodynamic flow and heat transfer over a permeable stretching sheet with slip condition. In a similar way, Aziz [7] studied hydrodynamic and thermal slip boundary layer flow over a flat plate with constant heat flux boundary condition. The above mentioned literature discussed the slip boundary conditions when the first order velocity slip boundary conditions were used. However, Fang et al. [8] found a closed form solution for viscous flow over a shrinking sheet using the second order velocity slip flow model. Similarly, Mahantesh et al. [9] studied flow and heat transfer over a stretching sheet by considering second order velocity slip boundary condition.

Nanofluids are the suspension of nanometer-sized solid particles and fibers, which have been proposed as a means for enhancing the performance of heat transfer liquids currently available, such as water, toluene, oil and ethylene glycol mixture. Nanofluids have received the interest of many researchers recently because of their greatly enhanced thermal conductivity property [10]. One can refer the works of authors [11–13] regarding the thermal conductivity enhancement of the nanofluids available in the literature. Nowadays, the study of convective heat transfer in nanofluids become active research area due to its heat transfer enhancement characteristics. Because of the fact that cooling is one of the technical challenges faced many industries including microelectronic, transportation, solid-state lighting and manufacturing; the idea of nanofluid has been proposed as a means of alleviating these challenges.

The boundary layer flow and heat transfer due to nanofluids over a stretching sheet are a thrust areas of current research. Such investigations find applications over a broad spectrum of science and engineering disciplines. An important aspect of boundary layer flow of a nanofluid over a stretching sheet is the heat transfer characteristics. It is crucial to understand the heat transfer characteristics of the stretching sheet so that the finished product meets the desired quality. This is due to the fact that the quality of a final product depends on the rate of heat transfer at the stretching surface. Accordingly, Kuznetsov and Nield [14] have studied the natural convective boundary-layer flow of a nanofluid past a vertical plate analytically. They used a model in which Brownian motion and thermophoresis effects were taken into account. Moreover, Khan and Pop [15] used the same model to study the boundary layer flow of a nanofluid past a stretching sheet with a constant surface temperature. Very recently Ibrahim and Shanker [16] have studied the boundary-layer flow and heat transfer of nanofluid over a vertical Plate taking into account the convective surface boundary condition. Recently, Haddad et al. [17] experimentally

investigated natural convection in nanofluid by considering the role of thermophoresis and Brownian motion in heat transfer enhancement. They indicated that neglecting the role of Brownian motion and thermophoresis deteriorate the heat transfer and this deterioration elevates when the volume fraction of a nanoparticles increases.

Similarly, Bachok et al. [18] numerically studied steady boundary layer flow of a nanofluid over a moving semi-infinite plate in a uniform free stream. Further, Makinde and Aziz [19] conducted a numerical study of boundary layer flow of a nanofluid past a stretching sheet with convective boundary condition. Also, Vajravelu et al. [20] discussed the convective heat transfer in a nanofluid flow over a stretching surface using Ag–water or Cu–water nanofluid. Furthermore, Hamad and Ferdows [21] studied boundary layer stagnation point flow towards a heated porous stretching sheet saturated with a nanofluid with heat absorption/generation and suction/blowing using Lie group analysis. Similarly, Mustafa et al. [22] investigated stagnation point flow of a nanofluid towards a stretching sheet. Wubshet et al. [23] were also numerically investigated the MHD stagnation point flow of a nanofluid towards a stretching sheet. Moreover, magnetic effects on free convection flow of a nanofluid past a vertical semi-infinite flat plate have been discussed by Hamad et al. [24]. Still, Yacob et al. [25] have further analyzed the boundary layer flow and heat transfer applying a convective boundary condition to the problem of flow over flat plate. MHD slip flow, heat and mass transfer in nanofluids over a permeable stretching/shrinking surface analytically studied by [26]. Moreover, Uddin et al. [27] analyzed scaling group transformation for MHD boundary layer slip flow of a nanofluid over a convectively heated stretching sheet with heat generation.

The comprehensive review of nanofluids about theoretical and numerical investigation, experiments and applications were described by Wang and Mujumdar [28,29]. They discussed the theoretical investigation, preparation and applications of the nanofluids. An interested reader can refer to these reviews.

The aforesaid studies analyzed the boundary layer flow of nanofluids by neglecting the slip boundary condition in the flow analysis. Very recently, Aminreza et al. [30] and Kalidas [31] numerically investigated the effect of partial slip boundary condition on the flow and heat transfer of a nanofluid past a stretching sheet. They indicated that the reduced Nusselt number and Sherwood number are strongly influenced by the slip parameter.

All the above studies considered the no-slip thermal and solutal boundary condition. But, there might be a natural situation where no-slip boundary condition may not be applicable. In such circumstances, we may be forced to consider slip boundary condition.Therefore, this study try to fulfil this gap. In this paper we considered the slip boundary conditions in velocity, temperature and concentration to study the boundary layer flow and heat transfer analysis of a nanofluid. Hence, the purpose of this study is to fill this felt out knowledge gap in the nanofluid. The study analyzes magnetohydrodynamics boundary layer flow over a stretching sheet in nanofluid with the inclusion of radiation effect. Moreover, the combined effects of Brownian motion, thermophoresis parameter and nanoparticle fraction on boundary layer flow and heat transfer due to nanofluid are examined.

2. Mathematical formulation

Consider a two-dimensional steady state boundary layer flow of a nanofluid over stretching sheet with surface temperature T_w and concentration C_w. The stretching velocity of the sheet is $u_w = ax$, with a being a constant. Let the wall mass transfer be V_w, which will be determined later. The flow is assumed to be generated by stretching sheet issuing from a thin slit at the origin. The sheet is then stretched in such a way that the speed at any point on the sheet becomes proportional to the distance from the origin. The ambient temperature and concentration, respectively, are T_∞ and C_∞. The flow is subjected to the combined effect of thermal radiation and a transverse magnetic field of strength B_0, which is assumed to be applied in the positive y-direction, normal to the surface. The induced magnetic field is also assumed to be small compared to the applied magnetic field; so it is neglected. It is further assumed that the base fluid and the suspended nanoparticles are in thermal equilibrium. It is chosen that the coordinate system x-axis is along stretching sheet and y-axis is normal to the sheet.

Under the above assumptions, the governing equation of the conservation of mass, momentum, energy and nanoparticles fraction in the presence of magnetic field and thermal radiation past a stretching sheet can be expressed as:

$$\frac{\partial u}{\partial x}+\frac{\partial v}{\partial y}=0 \tag{1}$$

$$u\frac{\partial u}{\partial x}+v\frac{\partial u}{\partial y}=-\frac{1}{\rho_f}\frac{\partial p}{\partial x}+\upsilon\left(\frac{\partial^2 u}{\partial x^2}+\frac{\partial^2 u}{\partial y^2}\right)-\frac{\sigma B_0^2}{\rho_f}u \tag{2}$$

$$u\frac{\partial v}{\partial x}+v\frac{\partial v}{\partial y}=-\frac{1}{\rho_f}\frac{\partial p}{\partial y}+\upsilon\left(\frac{\partial^2 v}{\partial x^2}+\frac{\partial^2 v}{\partial y^2}\right)-\frac{\sigma B_0^2}{\rho_f}v \tag{3}$$

$$u\frac{\partial T}{\partial x}+v\frac{\partial T}{\partial y}=\alpha\left(\frac{\partial^2 T}{\partial x^2}+\frac{\partial^2 T}{\partial y^2}\right)-\frac{1}{(\rho c)_f}\left(\frac{\partial q_r}{\partial y}\right)+\frac{\mu}{\rho c_p}\left(\frac{\partial u}{\partial y}\right)^2+\left(\frac{\sigma B_0^2}{\rho c_p}\right)u^2+\tau\left\{D_B\left(\frac{\partial\phi}{\partial x}\frac{\partial T}{\partial x}+\frac{\partial\phi}{\partial y}\frac{\partial T}{\partial y}\right)+\frac{D_T}{T_\infty}\left[\left(\frac{\partial T}{\partial x}\right)^2+\left(\frac{\partial T}{\partial y}\right)^2\right]\right\} \tag{4}$$

$$u\frac{\partial\phi}{\partial x}+v\frac{\partial\phi}{\partial y}=D_B\left(\frac{\partial^2\phi}{\partial x^2}+\frac{\partial^2\phi}{\partial y^2}\right)+\frac{D_T}{T_\infty}\left(\frac{\partial^2 T}{\partial x^2}+\frac{\partial^2 T}{\partial y^2}\right) \tag{5}$$

where ρ_f, σ, B_0, ρ_p, $(c\rho)_f$, D_B and D_T are the density of the base fluid, electrical conductivity, magnetic field, the density of the nanoparticle, heat capacity of a fluid, the Brownian diffusion and thermophoresis diffusion coefficient respectively. The boundary conditions are:

$$\begin{aligned}&u=u_w+L\frac{\partial u}{\partial y},\quad v=V_w,\quad T=T_w+K_1\frac{\partial T}{\partial y},\\&C=C_w+K_2\frac{\partial C}{\partial y},\quad \text{at}\quad y=0\\&u\to U_\infty=0,\quad T\to T_\infty,\quad C\to C_\infty\quad \text{as}\quad y\to\infty\end{aligned} \tag{6}$$

where $u_w=ax, T_w=T_\infty+b\left(\frac{x}{l}\right)^2, C_w=C_\infty+C\left(\frac{x}{l}\right)^2$, L, K_1 and K_2 are the velocity, the thermal and concentration slip factor, respectively, and when $L = K_1 = K_2 = 0$, the no-slip condition is recovered, l is reference length of a sheet. The above boundary condition is valid when $x \ll l$ which occurs very near to the slit.

Using an order magnitude analysis of the y-direction momentum equation (normal to the sheet) and the usual boundary layer approximations, such as:

$$\begin{aligned}&u\gg v\\&\frac{\partial u}{\partial y}\gg\frac{\partial u}{\partial x},\frac{\partial v}{\partial x},\frac{\partial v}{\partial y}\\&\frac{\partial p}{\partial y}=0\end{aligned} \tag{7}$$

After boundary-layer approximation, the governing equations are reduced to:

$$\frac{\partial u}{\partial x}+\frac{\partial v}{\partial y}=0 \tag{8}$$

$$u\frac{\partial u}{\partial x}+v\frac{\partial u}{\partial y}=\upsilon\left(\frac{\partial^2 u}{\partial y^2}\right)-\frac{\sigma B_0^2}{\rho_f}u \tag{9}$$

$$u\frac{\partial T}{\partial x}+v\frac{\partial T}{\partial y}=\alpha\left(\frac{\partial^2 T}{\partial y^2}\right)-\frac{1}{(\rho c)_f}\left(\frac{\partial q_r}{\partial y}\right)+\frac{\mu}{\rho c_p}\left(\frac{\partial u}{\partial y}\right)^2+\left(\frac{\sigma B_0^2}{\rho c_p}\right)u^2+\tau\left\{D_B\frac{\partial \phi}{\partial y}\frac{\partial T}{\partial y}+\frac{D_T}{T_\infty}\left[\left(\frac{\partial T}{\partial y}\right)^2\right]\right\} \tag{10}$$

$$u\frac{\partial \phi}{\partial x}+v\frac{\partial \phi}{\partial y}=D_B\frac{\partial^2 \phi}{\partial y^2}+\frac{D_T}{T_\infty}\frac{\partial^2 T}{\partial y^2} \tag{11}$$

The boundary conditions are:

$$u=u_w+L\frac{\partial u}{\partial y},\quad v=V_w,\quad T=T_w+K_1\frac{\partial T}{\partial y},$$
$$C=C_w+K_2\frac{\partial C}{\partial y},\quad \text{at}\quad y=0$$
$$u\to U_\infty=0,\quad T\to T_\infty,\quad C\to C_\infty\quad \text{as}\quad y\to\infty \tag{12}$$

where $\alpha=\frac{k}{(c\rho)_f}$, $\tau=\frac{(c\rho)_p}{(c\rho)_f}$, $\upsilon=\frac{\mu}{\rho_f}$, x and y represent coordinate axes along the continuous surface in the direction of motion and normal to it, respectively. The velocity components along x and y-axis are u and v respectively. υ is the kinematic viscosity, T is the temperature inside the boundary layer, $(c\rho)_p$ effective heat capacity of a nanoparticle, ρ is the density, T_∞ is the temperature far away from the sheet.

Introducing the following dimensionless quantities, the mathematical analysis of the problem is simplified by using similarity transforms:

$$\eta=\sqrt{\frac{a}{\upsilon}}y,\quad \psi=\sqrt{a\upsilon}xf(\eta),\quad \theta(\eta)=\frac{T-T_\infty}{T_w-T_\infty},$$
$$\phi(\eta)=\frac{C-C_\infty}{C_w-C_\infty} \tag{13}$$

The equation of continuity is satisfied if a stream function $\psi(x,y)$ is chosen as:

$$u=\frac{\partial \psi}{\partial y},\qquad v=-\frac{\partial \psi}{\partial x} \tag{14}$$

The radiative heat flux in the x-direction is considered negligible as compared to y-direction. Hence, by using Rosseland approximation for radiation, the radiative heat flux q_r is given by

$$q_r=-\frac{4\sigma^*}{3k^*}\frac{\partial T^4}{\partial y} \tag{15}$$

where σ^* and k^* are the Stefan–Boltzmann constant and the mean absorption coefficient, respectively. We assume that the temperature difference with in the flow is sufficiently small such that the term T^4 may be expressed as a linear function of temperature. This is done by expanding T^4 in a Taylor series about a free stream temperature T_∞ as follows:

$$T^4=T_\infty^4+4T_\infty^3(T-T_\infty)+6T_\infty^2(T-T_\infty)^2+\cdots \tag{16}$$

Neglecting higher-order terms in the above Eq. (16) beyond the first order in $(T-T_\infty)$, we get:

$$T^4\cong 4T_\infty^3T-3T_\infty^4 \tag{17}$$

Thus, substituting Eq. (17) into Eq. (15), we get:

$$q_r=-\frac{16T_\infty^3\sigma^*}{3k^*}\frac{\partial T}{\partial y} \tag{18}$$

Using the similarity transformation quantities, the governing Eqs. (8)–(11) are transformed to the ordinary differential equation as follows:

$$f'''+ff''-f'^2-Mf'=0 \tag{19}$$

$$\left(1+\frac{4}{3}R\right)\theta''+\mathrm{Pr}f\theta'-2\mathrm{Pr}f'\theta+\mathrm{PrEc}f''^2+\mathrm{PrMEc}f'^2+\mathrm{PrNb}\phi'\theta'+\mathrm{PrNt}\theta'^2=0 \tag{20}$$

$$\phi''+\mathrm{Le}f\phi'-2\mathrm{Le}f'\phi+\frac{\mathrm{Nt}}{\mathrm{Nb}}\theta''=0 \tag{21}$$

With boundary conditions

$$f(0)=S,f'(0)=1+Af''(0),\theta(0)=1+B\theta'(0),$$
$$\phi(0)=1+C\phi'(0),\quad \text{at}\quad \eta=0,f'(\infty)=0,\quad \theta(\infty)=0,$$
$$\phi(\infty)=0,\quad \text{as}\quad \eta\to\infty \tag{22}$$

where the governing parameters are defined as:

$$\left.\begin{aligned}&\mathrm{Pr}=\tfrac{\upsilon}{\alpha}\\&Ec=\tfrac{u_w^2}{c_p(T_w-T_\infty)}\\&R=\tfrac{4\sigma^*T_\infty^3}{3k^*k}\\&M=\tfrac{\sigma B_0^2}{\rho_f a}\\&\mathrm{Nb}=\tfrac{(\rho c)_pD_B(\phi_w-\phi_\infty)}{(\rho c)_f\upsilon}\\&\mathrm{Nt}=\tfrac{(\rho c)_pD_T(T_w-T_\infty)}{(\rho c)_f\upsilon T_\infty}\\&\mathrm{Le}=\tfrac{\upsilon}{D_B}\\&A=L\sqrt{\tfrac{a}{\upsilon}}\\&B=K_1\sqrt{\tfrac{a}{\upsilon}}\\&C=K_2\sqrt{\tfrac{a}{\upsilon}}\end{aligned}\right\}\text{Governing parameters} \tag{23}$$

where f', θ and ϕ are the dimensionless velocity, temperature and nanoparticle concentration, respectively. η is the similarity variables, the prime denotes differentiation with respect to η. Pr, R, M, Ec, Nb, Nt, Le denote a Prandtl number, a radiation parameter, a magnetic parameter, Eckert number, a Brownian motion parameter, a thermophoresis parameter, and a Lewis number, respectively. A, B, C are velocity, thermal and concentration slip parameters, respectively.

The important physical quantities of interest in this problem are local skin friction coefficient c_f, the local Nusselt number Nu_x and the local Sherwood number Sh_x are defined as:

$$c_f=\frac{\tau_w}{\rho u_w^2},\quad \mathrm{Nu}_x=\frac{xq_w}{k(T_w-T_\infty)},\quad \mathrm{Sh}_x=\frac{xh_m}{D_B(\phi_w-\phi_\infty)} \tag{24}$$

Where the wall heat flux q_w and mass flux h_m are given by:

$$q_w=-k\left(\frac{\partial T}{\partial y}\right)_{y=0},\quad h_m=-D_B\left(\frac{\partial \phi}{\partial y}\right)_{y=0} \tag{25}$$

By using the above equations, we get:

$$c_f\sqrt{\mathrm{Re}_x}=-f''(0),\quad \frac{\mathrm{Nu}_x}{\sqrt{\mathrm{Re}_x}}=-(1+R)\theta'(0),\quad \frac{\mathrm{Sh}_x}{\sqrt{\mathrm{Re}_x}}=-h'(0)s \tag{26}$$

where c_f, Re_x, Nu_x, Sh_x are the skin friction, local Reynolds number, local Nusselt number and local Sherwood number, respectively.

3. Numerical solution

An efficient fourth order Runge–Kutta method along with shooting technique has been employed to study the flow model for the above coupled non-linear ordinary differential equations Eqs. (19)–(21) for different values of governing parameters viz. Prandtl number Pr, radiation parameter R, a Brownian motion parameter Nb, a thermophoresis parameter Nt, Eckert number Ec and a Lewis number Le. The non-linear differential equations are first decomposed into a system of first order differential equation.

The coupled ordinary differential Eqs. (19)–(21) are third order in f and second order in θ and ϕ which have been reduced to a system of seven simultaneous equations for seven unknowns. In order to numerically solve this system of equations using Runge–Kutta method, the solution requires seven initial conditions but two initial conditions in f one initial condition in each of θ and ϕ are known. However, the values of f', θ and ϕ are known at $\eta \to \infty$. These end conditions are utilized to produce unknown initial conditions at $\eta = 0$ by using shooting technique. The most important step of this scheme is to choose the appropriate finite value of η_∞. Thus to estimate the value of η_∞, we start with some initial guess value and solve the boundary value problem consisting of Eqs. (19)–(21) to obtain $f''(0)$, $\theta'(0)$ and $\phi'(0)$. The solution process is repeated with another larger value of η_∞ until two successive values of $f''(0)$, $\theta'(0)$ and $\phi'(0)$ differ only after desired significant digit. The last value η_∞ is taken as the finite value of the limit η_∞ for the particular set of physical parameters for determining velocity, temperature and concentration, respectively, are $f(\eta)$, $\theta(\eta)$ and $\phi(\eta)$ in the boundary layer. After getting all the initial conditions we solve this system of simultaneous equations using fourth order Runge–Kutta integration scheme. The value of η_∞ is selected to vary from 5 to 20 depending on the physical parameters governing the flow so that no numerical oscillation would occur. Thus, the coupled boundary value problem of third-order in f, second-order in θ and ϕ has been reduced to a system of seven simultaneous equations of first-order for seven unknowns as follows:

The Eqs. (19)–(21) can be expressed as:

$$f''' = -ff'' + f'^2 - Mf' \tag{27}$$

$$\theta'' = -\Pr\frac{(f\theta' - 2f'\theta + Ecf''^2 + MEcf'^2 + \mathrm{Nb}\phi'\theta' + \mathrm{Nt}\theta'^2)}{\left(1+\frac{4}{3}R\right)} \tag{28}$$

$$\phi'' = -\mathrm{Le}f\phi' + 2\mathrm{Le}f'\phi - \frac{\mathrm{Nt}}{\mathrm{Nb}}\theta'' \tag{29}$$

Now we can define new variables by the equations:

$$f_1 = f,\quad f_2 = f',\quad f_3 = f'',\quad f_4 = \theta,\quad f_5 = \theta',$$
$$f_6 = \phi,\quad f_7 = \phi' \tag{30}$$

The coupled higher order non-linear differential equations and the boundary conditions may be transformed to seven equivalent first order differential equations and boundary conditions, respectively, as given below:

$$\left.\begin{aligned} f_1' &= f_2\\ f_2' &= f_3\\ f_3' &= -f_1f_3 + f_2^2 - Mf_2\\ f_4' &= f_5\\ f_5' &= \Pr\frac{\left(-f_1f_5 + 2f_2f_4 - Ecf_3^2 - EcMf_2^2 - \mathrm{Nb}f_5f_7 - \mathrm{Nt}f_5^2\right)}{\left(1+\frac{4}{3}R\right)}\\ f_6' &= f_7\\ f_7' &= -\mathrm{Le}f_1f_7 + 2\mathrm{Le}f_2f_6 + \frac{\mathrm{Nt}}{\mathrm{Nb}}\Pr\frac{\left(f_1f_5 - 2f_2f_4 + Ecf_3^2 + EcMf_2^2 + \mathrm{Nb}f_5f_7 + \mathrm{Nt}f_5^2\right)}{\left(1+\frac{4}{3}R\right)} \end{aligned}\right\}\ \text{System of equations} \tag{31}$$

A prime denote the differentiation with respect to η and the boundary conditions are:

$$f_1(0) = 0,\quad f_2(0) = 1 + Af_3(0),\quad f_4(0) = 1 + Bf_5(0),$$
$$f_6(0) = 1 + Cf_7(0)\quad f_2(\infty) = 0,\quad f_4(\infty) = 0,\quad f_6(\infty) = 0 \tag{32}$$

In this study, the boundary value problem is first converted into an initial value problem (IVP). Then the IVP is solved by appropriately guessing the missing initial value using the shooting method for several sets of parameters. The step size $h = 0.1$ is used for the computational purpose. The error tolerance of 10^{-7} is also being used. The results obtained are presented through tables and graphs, and the main features of the problems are discussed and analyzed.

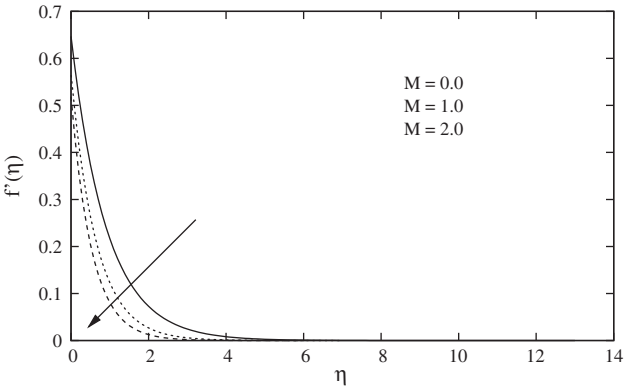

Fig. 1. Velocity graph for different values of M when Nb = Nt = 0.5, Le = 10, Pr = 10, $R = A = S = 0.5$.

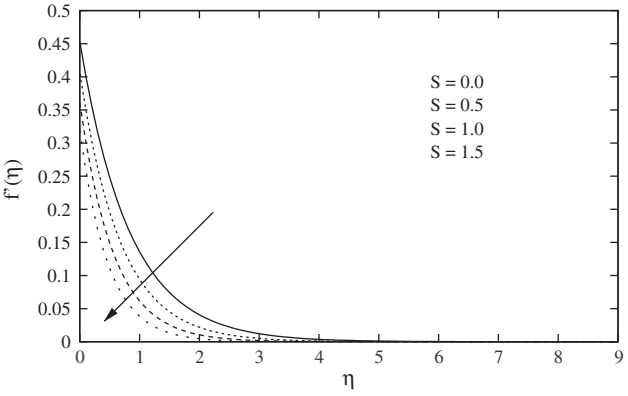

Fig. 2. Velocity graph for different values of suction parameter S when Nb = Nt = 0.5, Le = 10, Pr = 1, $A = M = 1$.

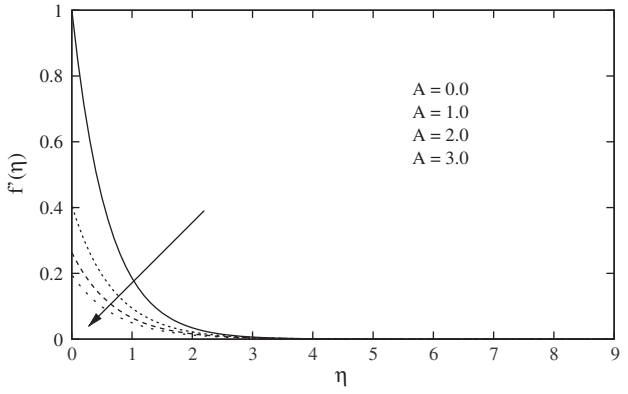

Fig. 3. Velocity graph for different values of velocity slip parameter A when Nb = Nt = 0.5, Le = 10, Pr = 1, $M = 1$, $S = 0.5$.

4. Results and discussion

The numerical solutions are obtained for velocity, temperature and concentration profiles for different values of governing parameters. The obtained results are displayed through graphs Figs. 1–16 for velocity, temperature and concentration profiles, respectively.

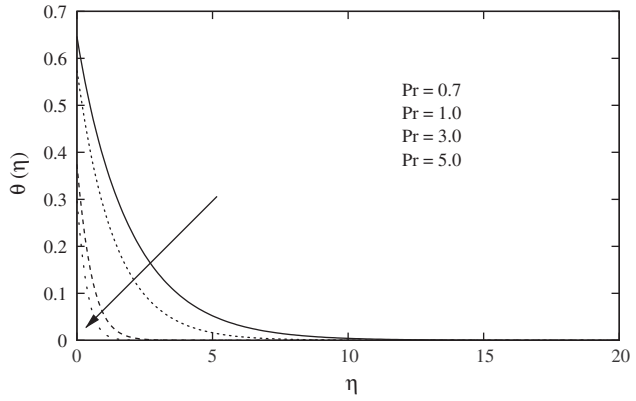

Fig. 4. Temperature graph for different values of Pr when Nb = Nt = R = 0.5, Le = 5, A = B = M = S = 1, Ec = 0.2.

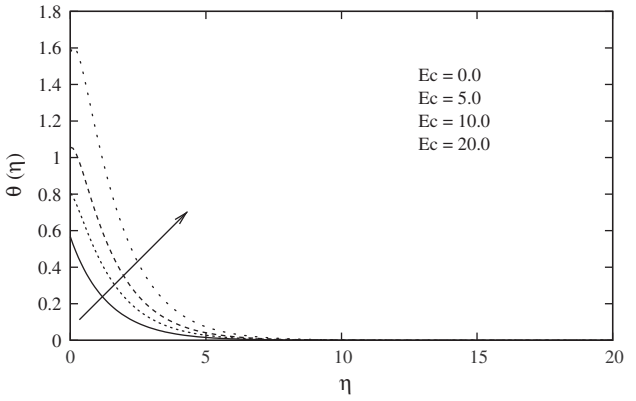

Fig. 7. Temperature graph for different values of Eckert number Ec when Nb = Nt = 0.5, R = 0.5, M = Pr = S = A = B = 1.

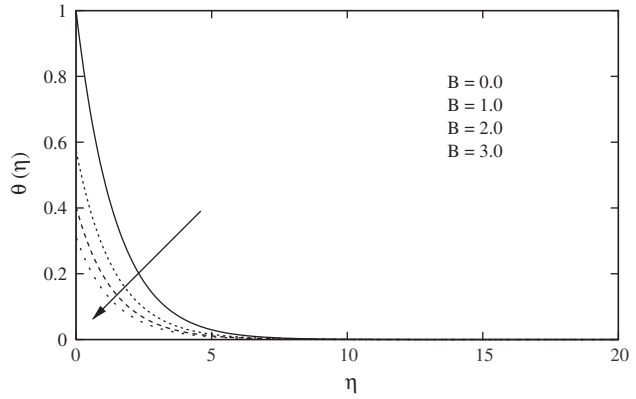

Fig. 5. Temperature graph for different values of thermal slip parameter B when Nb = Nt = 0.5, Ec = 0.2, R = 0.5, M = Pr = S = A = 1.

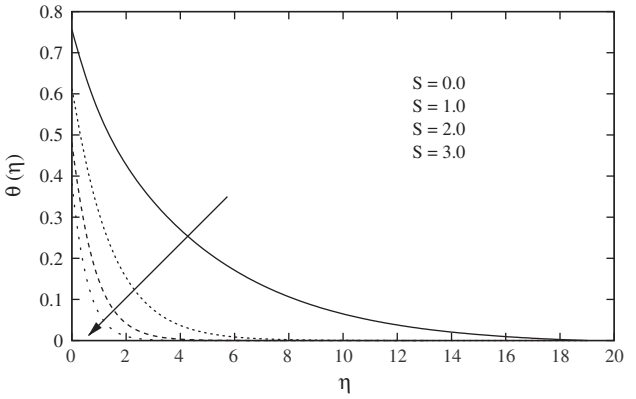

Fig. 8. Temperature graph for different values of suction parameter S when Nb = Nt = 0.5, R = 0.5, M = Pr = Ec = A = B = 1.

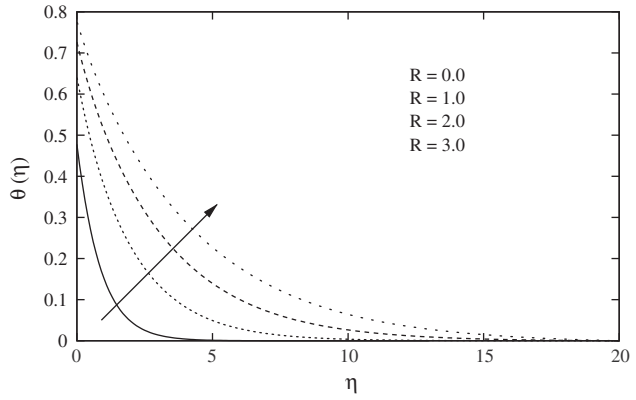

Fig. 6. Temperature graph for different values of Radiation parameter R when Nt = Nb = 0.5, M = S = B = A = 1, Pr = 10, Ec = 0.2.

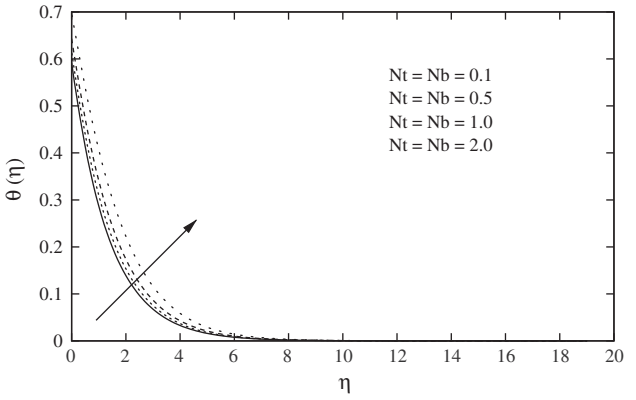

Fig. 9. Temperature graph for different values of Nb = Nt when M = Pr = S = A = B = 1, R = 0.5, Ec = 0.2.

Figs. 1–16 show that the far field boundary conditions are satisfied asymptotically, hence it supports the accuracy of the numerical result obtained. Moreover, the graphs for local Nusselt number and local Shrewood number are displayed through Figs. 17 and 18.

The velocity profile f' for different values of the magnetic field parameter M, mass suction parameter S and velocity slip parameter A are shown in Figs. 1–3, respectively.

Fig. 1 reveals the influences of magnetic field on the flow field. The presence of transverse magnetic field sets in Lorentz force effect, which results in the retarding effect on the velocity field. As the values of magnetic parameter M increase, the retarding force increases and consequently the velocity decreases. The graph also reveals that the boundary layer thickness reduces as magnetic parameter M increases. Figs. 2 and 3 display the distinction of velocity profile with respect to the variation in suction parameter S and velocity slip parameters A. On observing these figures, as the values of 'S' increase, the velocity profile graph decreases. Similarly, the velocity graph decreases as the values of velocity slip parameter A increase.

Figs. 4–11 present the variation of temperature with respect to the governing parameters, viz. Prandtl number Pr, thermal slip

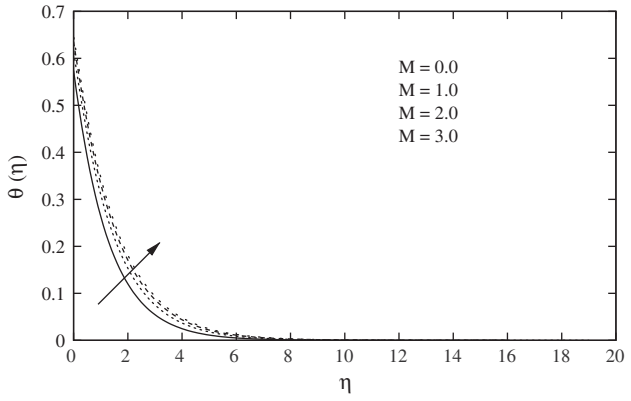

Fig. 10. Temperature graph for different values of M when Nb = N = 0.5t, M = Pr = S = A = B = 1, R = 0.5, Ec = 0.2.

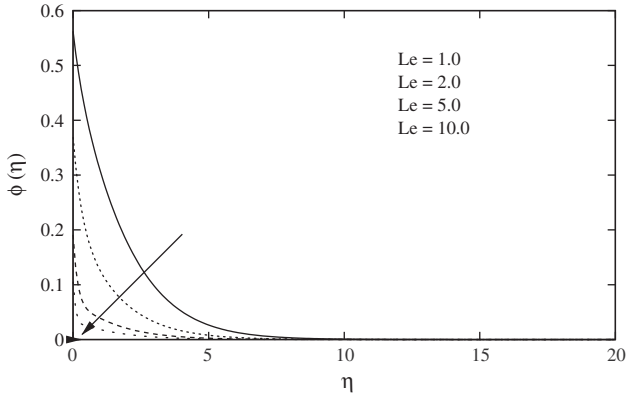

Fig. 11. Concentration graph for different values of Le when M = S = Ec = - Pr = A = B = C = 1, Nt = Nb = 0.5, R = 0.5.

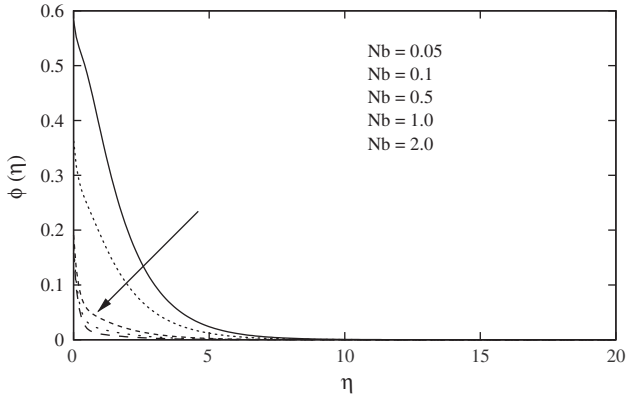

Fig. 12. Concentration graph for different values of Nb when Nt = 0.5, Le = 5, M = S = Ec = Pr = A = B = C = 1, R = 0.5.

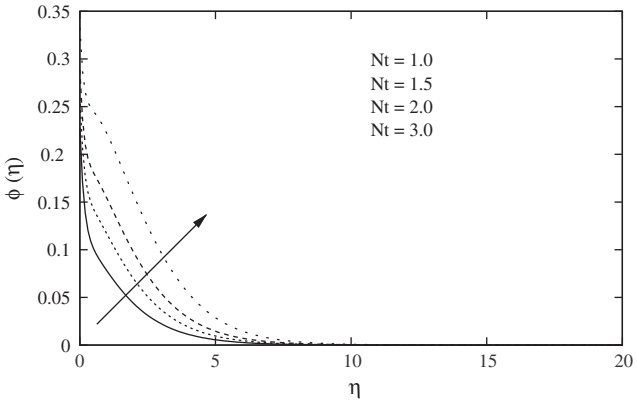

Fig. 13. Concentration graph for different values of Nt when M = S = Ec = - Pr = A = B = C = 1, Nb = 0.5, Le = 5, R = 0.5.

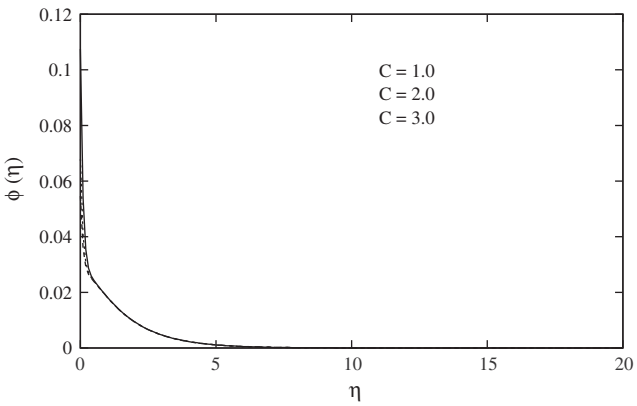

Fig. 14. Concentration graph for different values of solutal slip parameter when M = S = Ec = Pr = A = B = 1, Le = 10, Nt = Nb = 0.5, R = 0.5.

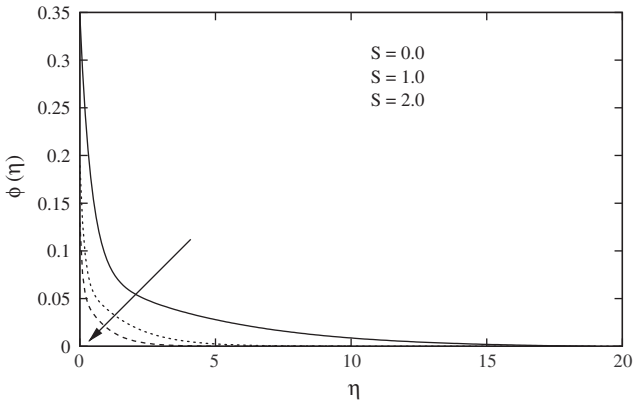

Fig. 15. Concentration graph for different values of suction parameter S when M = Ec = Pr = A = B = C = 1, Le = 5, Nt = Nb = 0.5, R = 0.5.

parameter B, radiation parameter R, Eckert number Ec, suction parameter S, thermophoresis parameter Nt and magnetic parameter M, respectively.

The effect of Prandtl number Pr on the heat transfer process is shown by the Fig. 4. This figure reveals that an increase in Prandtl number Pr results in a decrease in the temperature distribution, because, thermal boundary layer thickness decreases with an increase in Prandtl number Pr. In short, an increase in the Prandtl number means slow rate of thermal diffusion. The graph also shows that as the values of Prandtl number Pr increase, the wall temperature decreases. The effect of Prandtl on a nanofluid is similar to what has already been observed in common fluids qualitatively but they are different quantitatively. Therefore, these properties are inherited by nanofluids.

Fig. 5 shows the variation of temperature with respect to thermal slip parameter B. The graph reveals that the wall temperature $\theta(0)$ and thermal boundary layer thickness decreases when the values of B increases. However, the opposite effect is true with the radiation parameter R as shown in Fig. 6. As the values of R

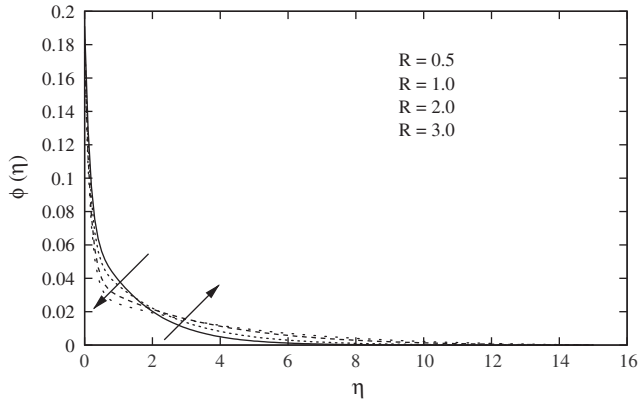

Fig. 16. Concentration graph for different values of radiation parameter R when $S = M = \mathrm{Ec} = \mathrm{Pr} = A = B = C = 1$, Le = 5, Nt = Nb = 0.5.

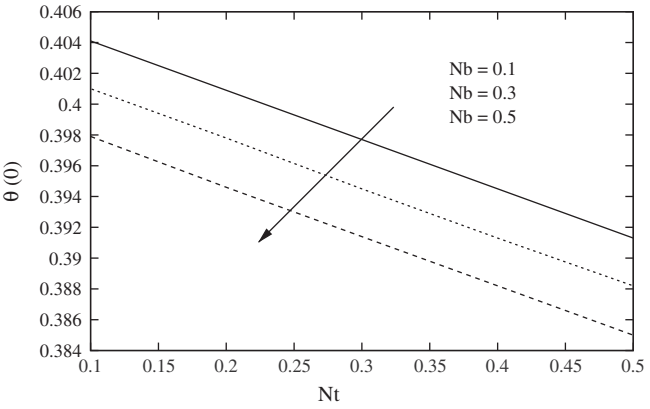

Fig. 17. Variation of local Nusselt number $-\theta'(0)$ with Nt for different values of Nb when Le = 10, Pr = 1.

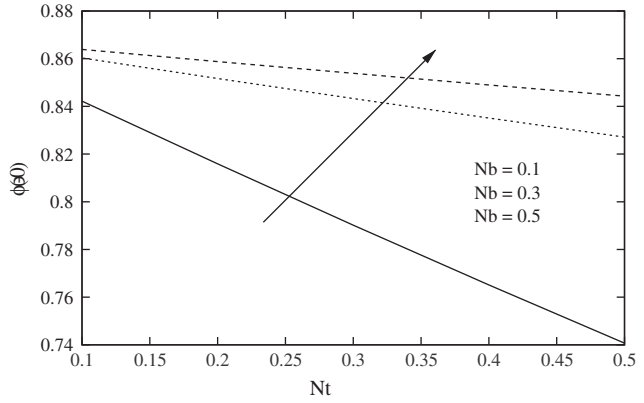

Fig. 18. Variation of local Sherwood number $-\phi'(0)$ with Nt for different values of Nb when Le = 10, Pr = 1.

increase, the thermal boundary layer thickness increases. This may be due to the reduction of rate of heat transfer at the surface as revealed in Table 4.

Fig. 7 illustrates the influence of Eckert number Ec on temperature in the boundary layer. On observing the temperature graph, the wall temperature of the sheet increases as the values of Ec increase. Moreover, when the values of Ec increase, the thermal boundary layer thickness increases. This is due to the fact that the heat transfer rate at the surface decrease as Ec increases as shown in Table 4.

Fig. 8 displays the variation of temperature with suction parameter S. As the values of suction parameter S increase, the temperature graph is decreasing. Moreover, the thermal boundary layer thickness and surface temperature is also decreasing.

Fig. 9 shows the influence of the change of Brownian motion parameter Nb and thermophoresis parameter Nt on temperature profile when (Nb = Nt). It is noticed that as thermophoesis parameter increases the thermal boundary layer thickness increases and the temperature gradient at the surface decrease (in absolute value) as both Nb and Nt increase. Therefore, the local Nusselt number $-\theta'(0)$, which represents the heat transfer rate at the surface, decreases. Consequently, temperature on the surface of a sheet increases. This is due to the fact that the thermophoresis Parameter Nt is directly proportional to the heat transfer coefficient associated with the fluid.

Fig. 10 shows the influence of magnetic field parameter M on the thermal field. Transverse magnetic field has increased the thermal boundary layer thickness. However, an increment in thermal boundary layer is not significant amount. Similar to other common fluids, the nanofluid shows similar characteristics regarding the influences of magnetic field on thermal field.

Figs. 11–15 demonstrate the variation of nanoparticle concentration with respect to the change in governing parameters, viz. Lewis number Le, Brownian motion parameter Nb, thermophoresis parameter Nt, concentration slip parameter, suction and radiation parameters.

As it is noticed from Fig. 11, as Lewis number increases the concentration graph decreases and the concentration boundary layer thickness decreases. This is probably due to the fact that mass transfer rate increases as Lewis number increases. It also reveals that the concentration gradient at surface of the sheet increases. Moreover, the concentration at the surface of a sheet decreases as the values of Le increase.

Graph Fig. 12 reveals the variation of concentration in response to a change in Brownian motion parameter Nb. As the values of Brownian motion parameter increase, the concentration boundary layer thickness is decreasing. Furthermore, the magnitude of concentration gradient on the surface of a sheet increases as the values of Nb increase. Thus, the local Sherwood number $-\phi'(0)$, which represents the mass transfer rate at the surface increases when Nb increases. This may be due to the fact that as a Brownian motion parameter Nb decreases the mass transfer of a nanofluid; consequently, mass transfer rate at a surface increases.

Graph Fig. 13 reveals variation of concentration graph in response to a change in thermophoresis parameter Nt. The influence of thermophoresis parameter on concentration profile graph is monotonic, i.e. as the values of Nt parameter increase, the concentration boundary layer thickness is also increasing. Moreover, it is possible to recognize from the graph that the magnitude of concentration gradient on the surface of a sheet decreases as the values Nt increase. Thus, the local Sherwood number $-\phi'(0)$, which represents the mass transfer rate at the surface decreases when Nt increases. This may be due to the fact that thermophoresis parameter Nt increases the mass transfer of a nanofluids; consequently, mass transfer rate at a surface decreases.

Fig. 14 illustrates the variation of concentration with respect to concentration slip parameter C. As it can be seen from the graph, the concentration slip parameter does not have any influences on concentration profile graph. On the other hand the suction parameter 'S' has a strong influence on the concentration profile as it is shown in Fig. 15. As the values of suction parameter S increase, concentration graph decreases and the concentration boundary layer thickness decreases.

Fig. 16 illustrates the variation of radiation on concentration graph. The influences of radiation parameter on concentration is not this much significant. As the values of radiation parameter R

increase, the concentration boundary layer thickness is not changing much. It can be observed from Table 4 that, as radiation parameter R increases, mass transfer rate is almost constant.

Fig. 17 shows that the influence of both the Brownian motion parameter Nb and thermophoresis parameter Nt on local Nusselt number $-\theta'(0)$. As both parameters increase, the heat transfer rate on the surface of a sheet decreases. This indicates that an increment in thermophoresis parameter induces resistance to the diffusion of mass. This results in the reduction of concentration gradient on the surface.

Fig. 18 also depicts the variation of local Sherwood number $-\phi'(0)$ in response to a change in Brownian motion parameter Nb. The graph shows that the local Sherwood number increases as Nb parameters increase but it decreases with an increase in Nt.

Finally, a comparison with previously published papers available in the literature has been done in order to check the accuracy of the present results. As it is shown in Tables 1 and 2, the numerical values of the skin friction coefficient $-f''(0)$ and local Nusselt number $-\theta'(0)$ in this paper for different values of A, S and Pr, are in excellent agreement with the result published in Andersson [2] and Hayat et al. [6]. Therefore, we are confident that our results are highly accurate to analyze this flow problem.

Table 2 presents the variation of the skin friction coefficient in relation to magnetic field, suction and velocity slip parameters. On observing this table, as both the values of magnetic field and suction parameters increase, the values of skin friction coefficient increase. However, the skin friction coefficient decreases as the values of velocity slip parameter increase. Table 3 shows the comparison of local Nusselt number $-\theta'(0)$ for different values of Prandtl number Pr and suction parameter S. It is possible to see that as both the values of Prandtl number Pr and suction parameter S increase, the heat transfer rate (local Nusselt number) is increasing. Table 4 elucidates the variation of the local Nusselt number and local Sherwood number with thermal and concentration slip parameters by fixing other governing parameters. As the values of thermal slip parameter B increase, the local Nusselt number $-\theta'(0)$ decreases, however, the local Sherwood number $-\phi'(0)$ increases and opposite effect is observed as the values of concentration slip parameter C increase. Table 5 represents the variation of both the heat transfer rate $-\theta'(0)$ and mass transfer rate $-\phi'(0)$ for different values of the parameters Nt, Nb and Le. As the values of Lewis number Le increase, both the values of $-\theta'(0)$ and $-\phi'(0)$ increase, but, opposite effect is observed as the values of Nt increase. As the values of Nb parameter increase, the values of $-\theta'(0)$ decrease but $-\phi'(0)$ decrease.

Table 1
Comparison of skin friction coefficient-f″(0) for different values of A when $S = M = 0$.

A	Andersson [2]	Hayat et al. [6]	Present result
0.0	1.0000	1.000000	1.0000
0.1	0.8721	0.872082	0.8721
0.2	0.7764	0.776377	0.7764
0.5	0.5912	0.591195	0.5912
2.0	0.2840	0.283981	0.2840
5.0	0.1448	0.144841	0.1448
10.0	0.0812	0.081249	0.0812
20.0	0.0438	0.043782	0.0438
50.0	0.0186	0.018634	0.0186

Table 2
Computed values of skin friction coefficient $-f''(0)$ for various values of M, S and A.

M	S	A	$-f''(0)$
0	0.5	0	1.2808
0.5			1.5000
1.0			1.6861
1.5			1.8508
2.0			2.0000
1.0	0		1.4142
	0.2		1.5177
	0.7		1.8069
	1.0		2.0000
	0.2	1	0.5656
		1.2	0.5055
		1.3	0.4801

Table 3
Comparison of local Nusselt number $-\theta'(0)$ at Nt = 0, Nb → 0, $M = R = A = B = 0$ for different values of Pr and S with previously published data when the power of $(\frac{x}{l})$ is equal to 1.

S	Pr	Hayat et al. [6]	Present result
−1.5	0.72	0.4570273	0.4570
	1	0.5000000	0.5000
	10	0.6451648	0.6542
0	0.72	0.8086314	0.8686
	1	1.0000000	1.0000
	3	1.9235913	1.9237
	10	3.7215968	3.7207
1.5	0.72	1.4943687	1.4944
	1	2.0000621	2.0000
	10	16.096248	16.0842

Table 4
Computation showing the values local Nusselt number $-\theta'(0)$ and Sherwood number $-\phi'(0)$ at Le = 5, $M = S = 1$, Nb = Nt = 0.5 for different values of Pr, R, B, C, Ec.

Pr	R	Ec	B	C	$-\theta'(0)$	$-\phi'(0)$
1	0.2	0.2	1	1	0.3616	0.6786
5					0.5473	0.6482
7					0.5696	0.6443
10					0.5869	0.6417
5	0.5				0.5246	0.6522
	0.7				0.5106	0.6546
	1.0				0.4139	0.6580
		1			0.3857	0.6870
		2			0.2513	0.7238
		3			0.1141	0.7609
		0.2	0		0.8872	0.6058
			1		0.4913	0.6580
			2		0.3295	0.6807
			1	0	0.4011	2.4949
				1	0.4913	0.6580
				2	0.5054	0.3788
				3	0.5111	0.2659

Table 5
Computation showing the local Nusselt $-\theta'(0)$ and Sherwood number $-\phi'(0)$ when $M = R = S = 0.5$, $A = B = C = 1$, Pr = 1, Ec = 0.2 for different values of Pr, Nt and Nb.

Le	Nt	Nb	$-\theta'(0)$	$-\phi'(0)$
5	0.2	0.2	0.3980	0.7448
10			0.3993	0.8427
15			0.4001	0.8847
20			0.4005	0.9085
5	0.1		0.4012	0.7679
	0.3		0.3947	0.7223
	0.4		0.3915	0.7002
	0.5		0.3884	0.6787
	0.2	0.1	0.4002	0.6971
		0.3	0.3957	0.7607
		0.4	0.3935	0.7687
		0.5	0.3913	0.7735

5. Conclusions

It has been theoretically analyzed the influence of various governing parameters viz. magnetic parameter M, thermal radiation parameter R, Prandtl number Pr, Brownian motion parameter Nb, suction parameter S, slip parameters (A,B,C), thermophoresis parameter Nt and Lewis number Le on flow field and heat transfer characteristics of the MHD boundary layer flow of a stretching sheet over a nanofluid. The numerical results obtained are in excellent agreement with the previously published data in limiting condition and for some particular cases of the present study. It is found that the magnitude of the local Nusselt number $-\theta'(0)$ decreases with both Le and Nt. Furthermore, the surface temperature $\theta(0)$ decreases with an increase in both Pr and B and the opposite effect is observed as the values of R and Ec increase. Similarly, the mass transfer rate at the surface $-\phi'(0)$ increases with an increase in Le and Nb.

The main findings of the study are summarized as follows:

1. Velocity profiles decrease with an increase in M.
2. The thickness of velocity boundary layer decreases with an increase in magnetic field parameter M.
3. The velocity at the surface of a sheet decreases as the values of A increase.
4. Thermal boundary layer thickness decreases with an increase in values of slip parameter B and Prandtl number Pr.
5. The thickness of thermal boundary layer increases with an increase in radiation parameter R, magnetic field parameter M and thermophoresis parameter Nt when Nt = Nb.
6. An increase in parameter Nb decreases the local Nusslet number $-\theta'(0)$ but the opposite is true in local Sherwood number $-\phi'(0)$.
7. The wall temperature gradient increases with an increase in Lewis Number Le and Prandtl number Pr.
8. The surface temperature of a sheet increases with radiation parameter R but it decreases with an increase in Prandtl number Pr.
9. Concentration boundary layer thickness decreases with an increase in parameter $V2$, Lewis number Le and Nb but increases with an increase in Nt.
10. The skin friction coefficient decreases as the values of velocity slip parameter A increases.

Acknowledgement

The authors wish to express their very sincere thanks to referees for their valuable comments and suggestions for the improvement of the manuscript.

References

[1] Sakiadis BC. Boundary layer behavior on continuous solid surface: II. The boundary layer on a continuous flat surface. J Am Ins Chem Eng 1961;7(2):221–5.
[2] Andersson H. Slip flow past a stretching surface. Acta Mech 2002;158:121–5.
[3] Wang CY. Flow due to a stretching boundary with partial slip-an exact solution of the Navier–Stokes equation. Chem Eng Sci 2002;57:3745–7.
[4] Wang CY. Stagnation slip flow and heat transfer on a moving plate. Chem Eng Sci 2006;61:7668–72.
[5] Fang T, Zhang J, Yao S. Slip MHD viscous flow over a stretching sheet – an exact solution. Commun Non-linear Sci Numer Simul 2009;14:3731–7.
[6] Hayat T, Qasim M, Mesloub S. MHD flow and heat transfer over permeable stretching sheet with slip conditions. Int J Numer Meth Fluid 2011;66:963–75.
[7] Aziz A. Hydrodynamic and thermal slip flow boundary layer over a flat plate with constant heat flux boundary condition. Commun Non-linear Sci Numer Simul 2010;15:573–80.
[8] Fang T, Yao S, Zhang J, Aziz A. Viscous flow over a shrinking sheet with second order slip flow model. Commun Non-linear Sci Numer Simul 2010;15:1831–42.
[9] Mahantesh M, Vajravelu K, Abel MS, Siddalingappa MN. Second order slip flow and heat transfer over a stretching sheet with non-linear Navier boundary condition. Int J Therm Sci 2012;58:142–50.
[10] Keblinski P, Eastman JA, Cahaill DG. Nanofluids for thermal transport. Mater Today 2005;8(6):36–44.
[11] Choi S. Enhancing thermal conductivity of fluids with nanoparticle. In: Development and applications of non-newtonian flow. ASME, FED-vol.231/MD-vol.66; 1995. p. 99–105.
[12] Eastman JA, Choi SUS, Li S, Yu W, Thompson LJ. Anomalously increased effective thermal conductivity of ethylene glycol-based nanofluids containing copper nanoparticles. Appl Phys Lett 2001;78(6):718–20.
[13] Choi SUS, Zhang ZG, Yu W, Lockwoow FE, Grulke EA. Anomalous thermal conductivities enhancement on nanotube suspension. Appl Phys Lett 2001;79:2252–4.
[14] kuznetsov AV, Nield DA. Natural convective boundary-layer flow of a nanofluid past a vertical plate. Int J Therm Sci 2010;49:243–7.
[15] Khan WA, Pop I. Boundary layer flow of a nanofluid past a stretching sheet. Int J Heat Mass Transfer 2010;53:2477–83.
[16] Ibrahim W, Shanker B. Boundary-layer flow and heat transfer of nanofluid over a vertical plate with convective surface boundary condition. J Fluid Eng-Trans ASME 2012:134. 081203-1.
[17] Haddad Z, Nada A, Oztop F, Mataoui A. Natural convection in nanofluids: are the thermophoresis and Brownian motion effect significant in nanofluids heat transfer enhancement? Int J Therm Sci 2012;57:152–62.
[18] Bachok N, Ishak A, Pop I. Boundary-layer flow of nanofluids over a moving surface in a flowing fluid. Int J Therm Sci 2010;49:1663–8.
[19] Makinde OD, Aziz A. Boundary layer flow of a nanofluid past a stretching sheet with convective boundary condition. Int J Therm Sci 2011;50:1326–32.
[20] Vajravelu K, Prasad KV, Jinho L, Changhoon L, Pop I, Robert A, et al. Convective heat transfer in the flow of viscous Ag–water and Cu–water nanofluids over a stretching surface. Int J Therm Sci 2011;50:843–51.
[21] Hamad A, Ferdows M. Similarity solution of boundary layer stagnation point flow towards a heated porous stretching sheet saturated with nanofluid with heat absorption/generation and suction/blowing: a lie group analysis. Commun Non-linear Sci Numer Simul 2012;17:132–40.
[22] Mostafa M, Hayat T, Pop I, Asghar S, Obaidat S. Stagnation point flow of a nanofluid towards a stretching sheet. Int J Heat Mass Transfer 2011;54:5588–94.
[23] Ibrahim W, Shanker B, Mahantesh M. MHD stagnation point flow and heat transfer due to nanofluid towards a stretching sheet. Int J Heat Mass Transfer 2013;56:1–9.
[24] Hamad MA, Pop I, Ismali AI. Magnetic field effects on free convection flow of a nanofluid past a vertical semi-infinite flat plate. Non-Linear Anal: Real World Appl 2011;12:1338–46.
[25] Yacob A, Ishak A, Pop I, Vajravelu K. Boundary layer flow past a stretching/shrinking surface beneath an external uniform shear flow with convective surface boundary condition in a nanofluid. Nanoscale Res Lett 2011;6(314):1–7.
[26] Turkyilmazoglu M. Exact analytical solution for heat and mass transfer of MHD slip flow in nanofluids. Chem Eng Sci 2012;84:182–7.
[27] Uddin MJ, Khan WA, Ismail AIMd. Scaling group transformation for MHD boundary layer slip flow of a nanofluid over a convectively heated stretching sheet with heat generation mathematical problems in engineering, vol. 2012. article ID 934964.
[28] Wang X, Mujumdar AS. A review on nanofluids – Part I: Theoretical and numerical investigation. Braz J Chem Eng 2008;25(04):613–30.
[29] Wang X, Mujumdar AS. A review on nanofluids-part ii: experiments and applications. Braz J Chem Eng 2008;25(04):631–48.
[30] Aminreza N, Pourajab R, Ghalambaz M. Effect of partial slip boundary condition on the flow and heat transfer of nanofluids past stretching sheet prescribed constant wall temperature. Int J Therm Sci 2012;54:253–61.
[31] Kalidas D. Slip flow and convective heat transfer of nanofluids over a permeable stretching surface. Comput Fluids 2012;64:34–42.